Journal of Materials Chemistry A

PAPER

View Article Online
View Journal | View Issue

Cite this: J. Mater. Chem. A, 2015, 3, 9817

Cr(VI) removal by magnetic carbon nanocomposites derived from cellulose at different carbonization temperatures†

Bin Qiu,[abc] Yiran Wang,[b] Dezhi Sun,*[a] Qiang Wang,[a] Xin Zhang,[d] Brandon L. Weeks,[d] Ryan O'Connor,[e] Xiaohua Huang,[e] Suying Wei*[c] and Zhanhu Guo*[b]

Received 13th February 2015
Accepted 20th March 2015

DOI: 10.1039/c5ta01227a

www.rsc.org/MaterialsA

Magnetic carbon nanoadsorbents fabricated by using cellulose and $Fe(NO_3)_3$ as the carbon and iron precursors have demonstrated great Cr(VI) removal performance. The magnetic carbon synthesized at a carbonization temperature of 700 °C and a heating rate of 10 °C min^{-1} (MC7–10) has a greater Cr(VI) removal capacity (22.8 mg g^{-1}) in neutral solutions due to its larger specific surface area (247.14 m^2 g^{-1}). Moreover, the magnetic carbon fabricated at a carbonization temperature of 800 °C and a heating rate of 10 °C min^{-1} (MC8–10) has the highest Cr(VI) removal capacity (278.8 mg g^{-1}) in acidic solutions, much higher than those of cellulose (12.0 mg g^{-1}), zero valent iron (ZVI)/chitosan (55.8 mg g^{-1}) and ZVI doped ordered mesoporous carbon (256.86 mg g^{-1}). The high removal capacity was attributed to its higher content of ZVI and specific surface area (136.27 m^2 g^{-1}) of MC8–10. The reduction of Cr(VI) to Cr(III) by the oxidation of carbon layer as well as the ZVI in the acidic solution was verified as the main mechanism for Cr(VI) removal. Moreover, the nanoadsorbents could be easily separated from solution by using a permanent magnet after being treated with Cr(VI).

1. Introduction

Chromium is a common contaminant in surface and ground water owing to its wide application in electroplating, printing, pigment and other industries.[1] Chromium is classified as one of the most toxic pollutants in wastewater.[2,3] The US Environmental Protection Agency (EPA) has issued a maximum concentration of 100 μg L^{-1} for total chromium according to the national primary drinking water regulations. A maximum allowable Cr(VI) concentration of 50 μg L^{-1} in drinking water is recommended by World Health Organization.

Among the reported various treatment methods, the adsorption is considered as the most popular method due to its low cost and high removal efficiency. As documented, Cr(VI) is acutely toxic, carcinogenic, highly soluble, and mobile in an aqueous environment. Contrarily, Cr(III) is relatively nontoxic and immobile.[4–6] It does not readily migrate in water since it is usually precipitated as hydroxides and oxides.[7] Therefore, the reduction of Cr(VI) to Cr(III) has been demonstrated to be important for Cr(VI) immobilization and its removal from wastewater.[4–6]

Various materials have been used as electron donors for this Cr(VI) reduction, such as zero-valent iron (ZVI),[8] Fe_3O_4,[8–11] zero-valent Al (ZVAl),[12] polymers[5,13] and cellulose.[4,6] The magnetic carbons, which have good magnetic properties, are widely used for Cr(VI) removal due to their reduction ability and adsorption ability, as well as their ease of separation from solutions after being used.[8–11] Magnetic carbons with ZVI core have been demonstrated to have much higher Cr(VI) removal capacity and faster removal rate, compared to the Fe_3O_4 and Fe_2O_3 core because ZVI can provide more electrons for Cr(VI) reduction.[14–17] Moreover, the carbon layer prevents the ZVI from dissolving in acidic solutions and from being oxidized by oxygen, leading to a longer life of the nanocomposites.[18] Carbon sources have been demonstrated crucial for the properties of the synthesized magnetic carbon, including the iron form and carbon layer. Many carbon precursors have been selected for fabricating magnetic carbons, such as polymers,[19] cotton,[20] furfuryl alcohol,[21] rice husk,[14] cellulose[15] and so on. Among these carbon sources, cellulose is the most abundant organic polymer in nature,[22] and is considered as a renewable and sustainable material for the preparation of carbon.[23–25]

Many methods, including the chemical vapor deposition method,[26] pyrolysis,[20,27] microwave assisted pyrolysis[19] and

[a]College of Environmental Science and Engineering, Beijing Forestry University, Beijing, 100083, China. E-mail: sundezhi@bjfu.edu.cn

[b]Integrated Composites Laboratory (ICL), Department of Chemical and Biomolecular Engineering, University of Tennessee, Knoxville, TN 37996, USA. E-mail: zguo10@utk.edu

[c]Department of Chemistry and Biochemistry, Lamar University, Beaumont, TX 77710, USA. E-mail: suying.wei@lamar.edu

[d]Department of Chemical Engineering, Texas Technology University, Lubbock, TX 79409, USA

[e]Department of Chemistry, The University of Memphis, Memphis, TN 38152, USA

† Electronic supplementary information (ESI) available. See DOI: 10.1039/c5ta01227a

hydrothermal carbonization method[28] have been developed to synthesize magnetic carbon. Among these methods, pyrolysis has been widely used due to its simple operation.[15,20,27] Gu *et al.*[19] has fabricated the magnetic carbon nanoadsorbents with the Fe_3O_4 core by using Fe_3O_4 and polyaniline as the iron and carbon precursors through calcination at a carbonization temperature of 750 °C and a rapid heating rate assisted with microwave. Zhu *et al.*[11] reported a magnetic carbon with ZVI/Fe_3O_4 core synthesized by using cotton fabric and $Fe(NO_3)_3$ as carbon and iron precursors *via* a calcination method at a carbonization temperature of 850 °C and a heating rate of 10 °C min^{-1}. Qiu *et al.*[15] synthesized a magnetic carbon by using cellulose and $Fe(NO_3)_3$ as carbon and iron precursors. Fe^{3+} was reduced to ZVI during the carbonization of cellulose at a final temperature of 800 °C and a heating rate of 10 °C min^{-1}. The properties of magnetic carbon, such as the iron form and specific surface area, highly affect Cr(VI) removal from polluted solutions. However, the effect of the carbonization conditions, including the carbonization temperature, heating rate and retention time, on the properties and Cr(VI) removal capacity of the synthesized magnetic carbon has not been reported yet.

In this study, magnetic carbon nanocomposites were fabricated by using cellulose and $Fe(NO_3)_3$ as the carbon and iron precursors *via* a simple calcination method. The effects of carbonization conditions, including the final carbonization temperature, heating rate and retention time, on the properties of the synthesized magnetic carbons were studied. Their Cr(VI) removal performance in neutral and acidic solutions were investigated. Meanwhile, the mechanisms involved in Cr(VI) removal from acidic and neutral solutions were disclosed to reveal the Cr(VI) removal nature of the magnetic carbon nanoadsorbents.

2. Materials and method

2.1. Materials

Cellulose and $Fe(NO_3)_3 \cdot 9H_2O$ were purchased from Sigma Aldrich. Potassium dichromate ($K_2Cr_2O_7$), 1,5-diphenylcarbazide (DPC) and ethanol were purchased from Alfa Aesar Company. Phosphoric acid (H_3PO_4, 85 wt%) was obtained from Fisher Scientific. All the chemicals were used as received without any further treatment.

2.2. Fabrication of magnetic carbon nanoadsorbents

20.0 g of $Fe(NO_3)_3 \cdot 9H_2O$ was dissolved in 200 mL of ethanol, and was mechanically stirred for 30 min. 2.0 g of cellulose was then mixed with the $Fe(NO_3)_3$ solution, and was stirred continuously for another 2 h, in order to make Fe^{3+} homogeneously distributed in cellulose. The mixtures were kept at room temperature for complete evaporation ofethanol . The remaining solid samples were then calcined at different final temperatures (600, 700, and 800 °C), different heating rates (2, 5 and 10 °C min^{-1}), and retention times (0, 30 and 60 min). The samples were named as MC*a*–*b*–*c*, and the "*a*", "*b*" and "*c*" were the carbonization temperature, heating rate and retention time, respectively. All the carbonization processes were conducted in nitrogen atmosphere.

2.3. Cr(VI) removal experiments

Cr(VI) removal performances by different magnetic carbons under acidic conditions were investigated by using magnetic carbon nanoadsorbents (50.0 mg) to treat 2.0 g L^{-1} Cr(VI) solutions (20.0 mL) at pH = 2.0 for 30 min. Their performances in neutral solution were also studied by using magnetic carbon nanoadsorbents (50.0 mg) to treat 50 mg L^{-1} Cr(VI) solutions (20.0 mL) at pH = 7.0 for 60 min. The equilibrium adsorption by the magnetic carbon can be achieved in 30 and 60 min respectively. The pH values of Cr(VI) solutions were adjusted by NaOH (1.0 mol L^{-1}) and H_2SO_4 (1.0 mol L^{-1}) with a pH meter (Vernier Lab Quest with pH-BTA sensor). All the Cr(VI) removal tests were conducted at room temperature.

The Cr(VI) concentration in solution was determined by the colorimetric method[7] by using the obtained standard fitting equation:

$$A = 9.7232 \times 10^{-4} C$$

where C is the Cr(VI) concentration, A is the absorbance at 540 nm obtained from the UV-vis test. The removal capacity (Q, mg g^{-1}) is quantified by eqn (1):

$$Q = \frac{(C_0 - C_e)V}{m} \quad (1)$$

where C_0 and C_e (mg L^{-1}) are the Cr(VI) concentrations in solution before and after being treated with magnetic carbon nanocomposites, respectively, V (L) represents the volume of Cr(VI) solution, m (g) is the dosage of the magnetic carbons used for Cr(VI) adsorption.

2.4. Characterization

The morphology of the fabricated magnetic carbons was characterized by scanning electron microscopy (SEM, Hitachi S4300). All the samples were sputter coated with a thin layer of gold (about 5 nm) to ensure good conductivity. The powder XRD analysis of the nanocomposites was carried out on a Bruker AXS D8 Discover diffractometer with GADDS (General Area Detector Diffraction System) operating with a Cu-Kα radiation source filtered with a graphite monochromator (λ = 1.5406 Å). The specific Brunauer–Emmett–Teller (BET) surface area was detected on a Quanta chrome Nova 2200e by nitrogen adsorption at 77.4 K. Prior to each measurement, the synthesized magnetic carbon samples were degassed at 300 °C for 12 h under high vacuum (<0.01 mbar). The pore size distribution of the nanocomposites was calculated by the Barrett–Joyner–Halenda (BJH) method using the nitrogen desorption isotherm. The X-ray photoelectron spectroscopy (XPS) measurements were conducted in the Kratos AXIS 165 XPS/AES instrument using a monochromatic Al K radiation to investigate the elemental composition. The Cr2p and C1s peaks were deconvoluted into the components consisting of a Gaussian/Lorentzian line shape function (Gaussian = 80%, Lorentzian = 20%) on a linear background. The Raman spectra were obtained using a Horiba Join-Yvon LabRam Raman confocal microscope with 785 nm laser excitation at a 1.5 cm^{-1} resolution at room temperature.

The magnetic properties were determined by using a 2 T physical property measurement system (PPMS) by Quantum Design at room temperature.

3. Results and discussion

3.1. Characterization

3.1.1 Final temperature. The SEM images of the magnetic carbons (Fig. 1) show that the particle becomes smaller and more uniform with increasing carbonization temperature. The irregular magnetic carbon nanoparticles were observed at a carbonization temperature of 600 °C (Fig. 1A), while uniform spherical particles with an average diameter of ~80 nm (Fig. 1C) were obtained at a carbonization temperature of 800 °C. The iron forms in the magnetic carbons fabricated at different carbonization temperatures were investigated by XRD (Fig. 2A). The diffraction peaks at 30.1°, 35.5°, 56.9° and 62.6° correspond to the (220), (311), (511) and (440) reflections of Fe_3O_4 (Fig. 2A(a & b)), respectively.[11] The diffractions peaks at 25.6°, 44.7° and 45.0° are indexed as the (002), (100) and (110) planes of the cubic ZVI.[11] The high intensity ratio of Fe_3O_4 to ZVI in MC6–10 and MC7–10 shows that Fe^{3+} has been transformed to Fe_3O_4 rather than reduced to ZVI at the carbonization temperatures of 600 and 700 °C. However, the ZVI peaks with high intensity in MC8–10 indicate that most Fe^{3+} has been reduced to ZVI by carbon at 800 °C.

The carbon structures of the magnetic carbons synthesized at different carbonization temperatures were characterized by Raman spectra (Fig. 3). The D-band peak at ~1293 cm^{-1} arising from the sp^3 C–C bond and G-band peak at ~1588 cm^{-1} arising from the C=C bond stretching vibrations were observed in all the magnetic carbons.[29,30] The D-band peak of the magnetic carbon shifts to a higher wavenumber, while the G-band peak shifts to a lower wavenumber with increasing carbonization temperature (Fig. 3A), indicating the interaction between the carbon and iron. The increased intensity ratio (I_D/I_G) of D-band

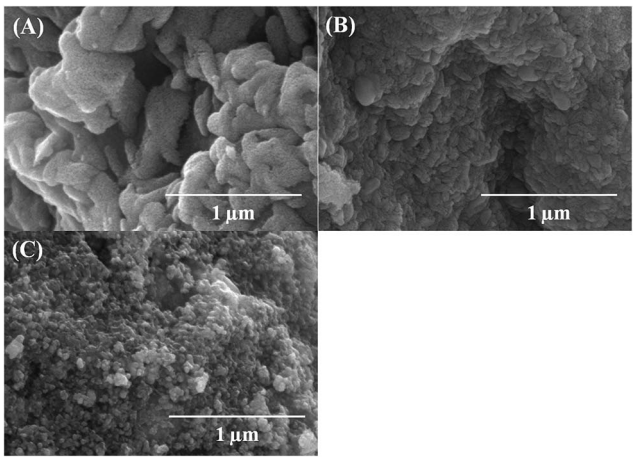

Fig. 1 SEM images of (A) MC6–10, (B) MC7–10 and (C) MC8–10.

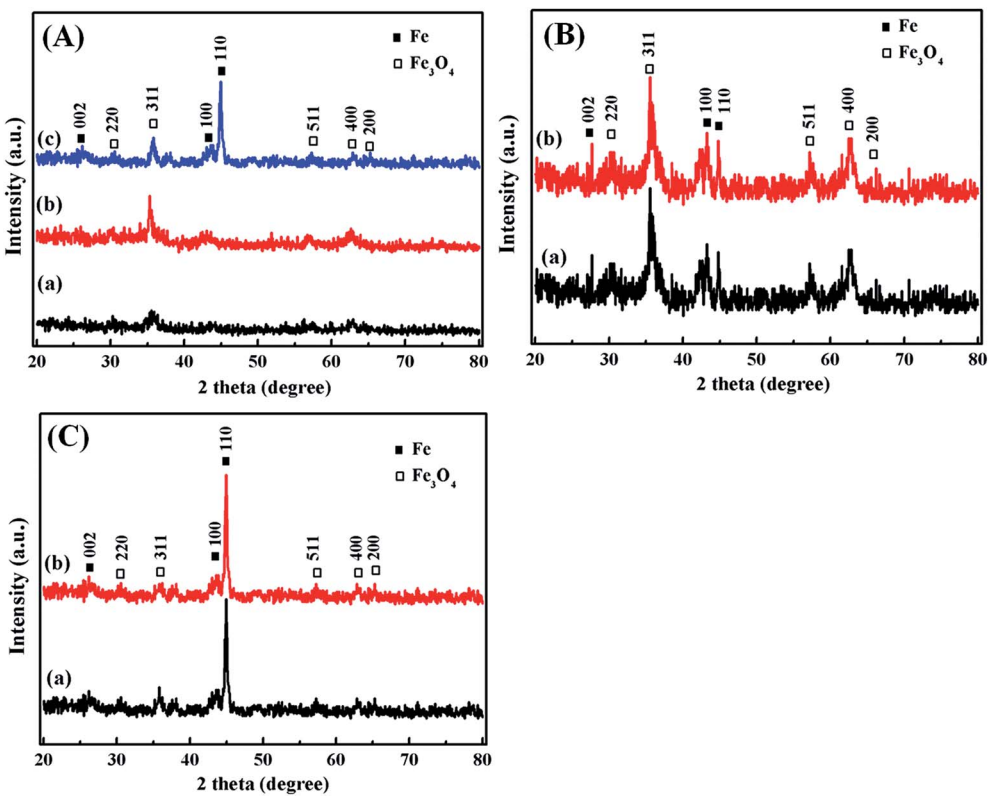

Fig. 2 XRD patterns of magnetic carbons synthesized (A) at carbonization temperatures of (a) 600, (b) 700 and (c) 800 °C (heating rate: 10 °C min^{-1}); (B) at heating rates of (a) 2 and (b) 5 °C min^{-1} (final temperature: 800 °C); and (C) with a retention time of (a) 30 and (b) 60 min (heating rate: 10 °C min^{-1}, final temperature: 800 °C).

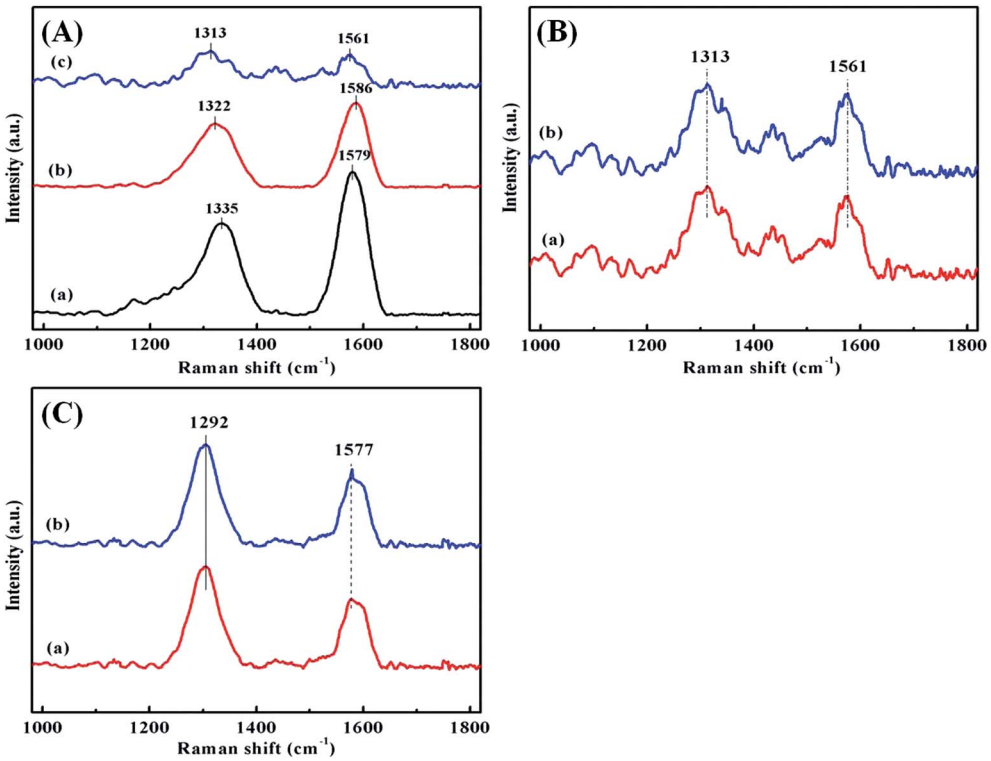

Fig. 3 Raman spectra of magnetic carbons synthesized (A) at carbonization temperatures of (a) 600, (b) 700 and (c) 800 °C (heating rate: 10 °C min^{-1}); (B) at heating rates of (a) 2 and (b) 5 °C min^{-1} (final temperature: 800 °C); and (C) with a retention time of (a) 30 and (b) 60 min (heating rate: 10 °C min^{-1}, final temperature: 800 °C).

to G-band with increasing final temperature (0.64, 0.76, 1.12) indicates a decrease in the size of the sp^2 domains.[31] In contrast to MC6–10 and MC7–10 (Fig. 3A(a & b)), the band peaks of MC8–10 are not well-defined (Fig. 3A(c)). The decreased peak intensities at 1313 and 1561 cm^{-1} and newly generated peaks at 1430 cm^{-1} indicate the interaction between the iron and carbon layer at the carbonization temperature of 800 °C.

The specific surface area and pore size distribution of the synthesized magnetic carbons were obtained by the nitrogen adsorption and desorption isotherms (Fig. 4A). The type-IV adsorption–desorption isotherm curves with the hysteresis loop indicate the mesoporous property of the nanocomposites. As shown in Table 1, the BET specific surface area of MC6–10, MC7–10 and MC8–10 are 241.58, 247.14 and 136.27 m^2 g^{-1}, respectively. The decreased specific surface area of MC8–10 indicates that carbon was consumed for Fe^{3+} reduction, consistent with the results based on XRD (Fig. 2A) and Raman spectral studies (Fig. 3A). The BJH pore size distribution calculated from the desorption branch is shown in Fig. 4A (inset). The pore size of magnetic carbon nanocomposites is centered at 3.9 nm with a narrow size distribution, which is contributed by the homogeneous distribution of iron nitrate with cellulose.

3.1.2 Temperature rate. MC8–5 and MC8–2 show uniform spherical particles with an average diameter of ~50 nm (Fig. S1†), a little smaller than that of MC8–10 (Fig. 1C). The increased particle size with increasing the heating rate indicates the aggregation of iron particles. The intensity ratio of Fe_3O_4 to ZVI of MC8–5 (Fig. 2B) and MC8–2 is much higher than that of MC8–10 (Fig. 2Ac), demonstrating that Fe^{3+} could not be reduced to ZVI when the heating rate was controlled at 2 and 5 °C min^{-1}. As shown in Fig. 3B, the band peaks of MC8–5 and MC8–2 are not well-defined, which are the same as MC8–10. The I_D/I_G ratios of MC8–5 and MC8–2 are 1.15 and 1.10, respectively, which are similar to that of MC8–10. The specific surface area decreases with increasing heating rate. More carbon was consumed for the Fe^{3+} reduction with a higher heating rate, consistent with the results from the XRD analysis that more ZVI was obtained with a heating rate of 10 °C min^{-1}. The pore sizes of MC8–5 and MC8–2 are centered at 3.9 nm (Fig. 4B), indicating that the pore size is not highly dependent on the heating rate.

3.2. Retention time

The bigger and more irregular particles of MC8–10–30 and MC8–10–60 (Fig. S2†) compared to MC8–10 indicate the aggregation of the magnetic carbon, leading to adecreased specific surface area. As shown in Fig. 2C, ZVI was observed as the main iron specimen in both MC8–10–30 and MC8–10–60. No obvious change was observed for the iron form in MC8–10–30 and MC8–10–60 compared to MC8–10 (Fig. 2Ac). The band peaks of MC8–10–30 and MC8–10–60 are well-defined (Fig. 3C) compared to that of MC8–10 (Fig. 3A(c)). The D-band peak of both MC8–10–30 and MC8–10–60 is observed to be shifted to a lower wavenumber (1292 cm^{-1}), while the G-band peak is shifted to a higher wavenumber (1577 cm^{-1}). These indicate the

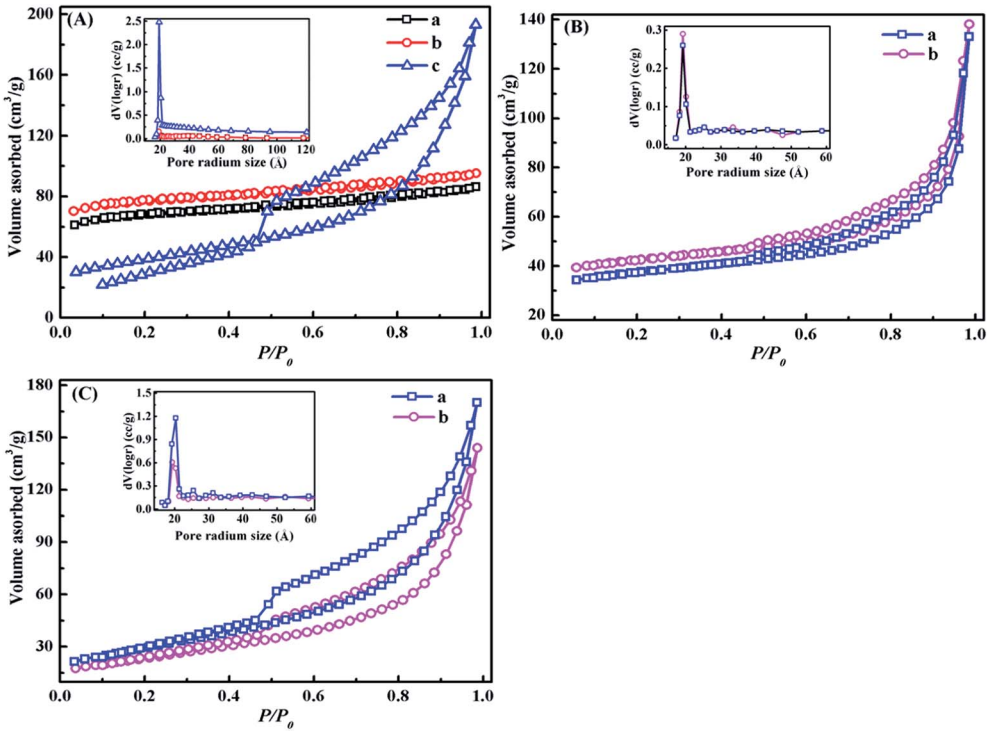

Fig. 4 N_2 adsorption–desorption isotherms and pore size distributions (inset) of magnetic carbons synthesized (A) at carbonization temperatures of (a) 600, (b) 700 and (c) 800 °C (heating rate: 10 °C min^{-1}); (B) at heating rates of (a) 2 and (b) 5 °C min^{-1} (final temperature: 800 °C); and (C) with a retention time of (a) 30 and (b) 60 min (heating rate: 10 °C min^{-1}, final temperature: 800 °C).

Table 1 Structural properties of magnetic carbons based on nitrogen adsorption/desorption isotherms

Samples	BET surface area (m^2 g^{-1})	Average pore size (nm)	Pore volume (cm^3 g^{-1})
MC6–10	241.58	3.90	0.044
MC7–10	247.14	3.90	0.052
MC8–10	136.27	3.90	0.325
MC8–5	144.67	3.90	0.187
MC8–2	156.34	3.90	0.192
MC8–10–30	114.58	3.90	0.262
MC8–10–60	82.94	3.82	0.218

interaction between the iron and the carbon during the retention period at 800 °C, leading to tight bonding between the iron core and carbon layer.[29,30] The I_D/I_G of MC8–10–30 and MC8–10–60 are 1.33 and 1.38 respectively. The slightly increased I_D/I_G ratio with increasing retention time demonstrates that part of the disordered carbon has been consumed for iron reduction. The representative type-IV nitrogen adsorption and desorption isotherm with the hysteresis loop (Fig. 4C) indicates the mesoporous structure of the magnetic carbons.[32] The specific surface area decreases with increasing retention time (104.58 and 84.94 m^2 g^{-1} for MC8–10–30 and MC8–10–60), further indicating that carbon has been consumed during the retention period. The pore size of MC8–10–30 is also centered at 3.9 nm, while the pore size of MC8–10–60 is decreased slightly to 3.8 nm. The consumption of carbon layer during the retention at 800 °C leads to a decreased specific surface area and pore size.

3.3. Cr(VI) removal

As shown in Fig. 5A, MC7–10 was observed to exhibit the highest adsorption capacity of 22.8 mg g^{-1} in the neutral solution, followed by MC6–10 (20.0 mg g^{-1}). No obvious difference in the adsorption capacity was observed for the magnetic carbons synthesized with different heating rates. However, the adsorption capacity decreased with increasing retention time. MC8–10–60 has the lowest adsorption capacity of 10.2 mg g^{-1}. These are consistent with the results of their specific surface area. The largest specific surface area of MC7–10 (247.14 m^2 g^{-1}) contributes to the highest Cr(VI) adsorption capacity while the decreased specific surface area with increasing retention time results in a decreased Cr(VI) adsorption capacity. The comparison of the Cr(VI) removal capacity by the synthesized magnetic carbons with other adsorbents is summarized in Table 2. The removal capacity of MC7–10 is much higher than those of the pristine cellulose (4.1 mg g^{-1}), active carbon (5.2 mg g^{-1}), magnetic carbon derived from cotton fabrics (3.73 mg g^{-1}),[11] and the nitrogen doped magnetic carbon derived from rice husk (15.6 mg g^{-1}).[14]

Here, MC7–10 was taken as an example to disclose the Cr(VI) removal mechanisms in neutral solution. The synthesized MC7–10 exhibits good magnetic properties with a saturation magnetization of 72.2 emu g^{-1} (Fig. S3†), and no obvious decreased magnetization was observed after being treated with the Cr(VI) solution at pH 7.0 (Fig. 5B), indicating that the carbon layer is stable and protects the Fe_3O_4 against dissolving in the solution. It also shows that the Fe_3O_4 in the magnetic carbon

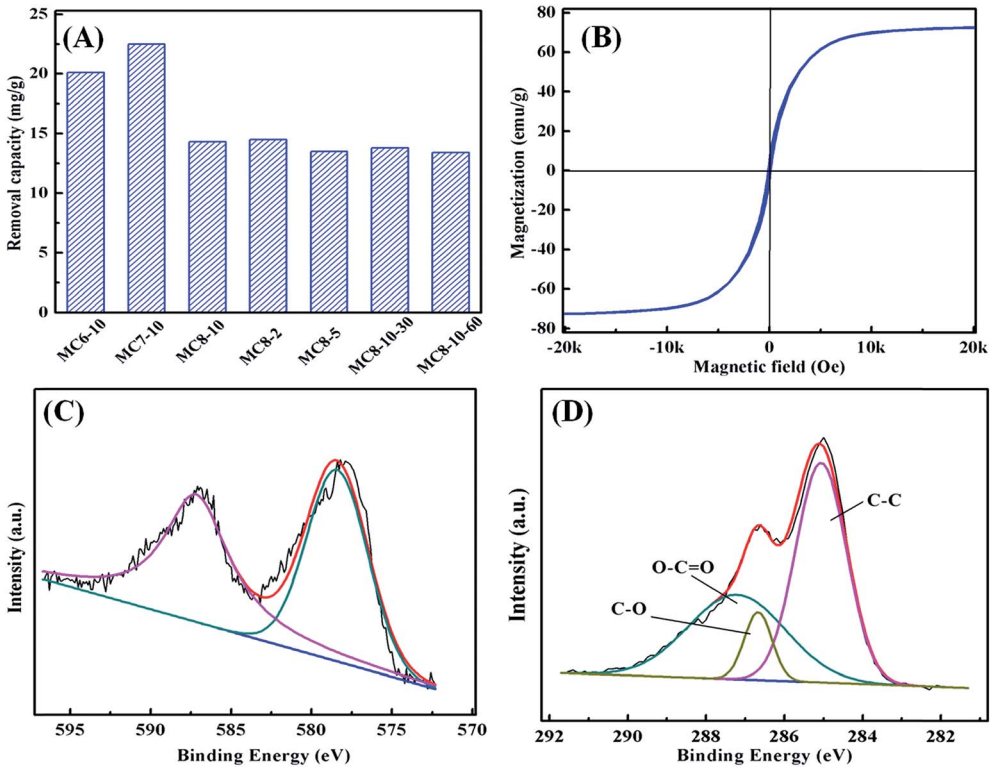

Fig. 5 (A) Cr(VI) removal by the synthesized magnetic carbons with an initial pH of 7.0; (B) magnetic hysteresis loop of MC8-10 after being treated with Cr(VI); (C) Cr2p and (D) C1s XPS spectra of MC8–10 after being treated with Cr(VI) solution.

Table 2 Comparison of Cr(VI) adsorption capacities with other adsorbents

Adsorbent	Adsorption capacity (mg g^{-1})	pH	Mechanism	References
Magnetic carbon	3.73	7.0	Reduction	11
Carbon fabrics	5.59	1.0	Reduction	3
Cellulose	12.0	1.0	Reduction	6
N-doped Fe_3O_4/carbon	16.0	3.0	Reduction	14
γ-Fe_2O_3 nanoparticles	19.2	2.5	Electrostatic interaction/ion exchange	36
δ-FeOOH-coated γ-Fe_2O_3	25.8	2.0	Electrostatic attraction	37
ZVI/chitosan	55.8	3.0	Reduction	34
ZVI nanoparticles	182	3.0	Reduction	38
ZVI/Fe_3O_4 nanoparticles	186.32	2.0	Reduction	16
ZVI/carbon	256.86	5.0	Reduction	17
ZVI/carbon	275.6	2.0	Reduction	This study

does not participate in the Cr(VI) removal process. The Fe_3O_4 particles in the adsorbent just act as the magnetic core, leading to easy separation of the adsorbent from solutions after being treated with Cr(VI). The larger specific surface area of MC7–10 facilitates Cr(VI) iron adsorption, indicating that Cr(VI) removal was mainly contributed by the carbon layer. The XPS was used to determine the reaction between Cr(VI) and the carbon of the magnetic carbon. As documented, the characteristic binding energy peaks at 577.0–580.0 eV and 586.0–588.0 eV correspond to Cr(III), and the peaks at 580.0–580.5 eV and 589.0–590.0 eV are contributed by Cr(VI).[33] Fig. 5C shows the XPS Cr2p spectra of MC7–10 after being treated with 100 mg L^{-1} of neutral Cr(VI) solution for 60 min. The binding energy peaks at 577.4 and 587.1 eV show the Cr(III) form of chromium on the surface of MC7–10, indicating that Cr(VI) was reduced to Cr(III). The C1s peak of the treated MC7–10 was deconvoluted to two major components with the binding energy peaks at 287.2, 286.6, 285.0 eV (Fig. 5D), which are related to the O–C=O, C–O and C–C. The new O–C=O group was generated after being treated with Cr(VI), compared to the C1s spectra of the synthesized MC7–10 (Fig. S4†). These indicate that Cr(VI) was completely reduced to Cr(III) by oxidation of carbon layer in the neutral solution.

The pH value has been demonstrated to be important for Cr(VI) removal by magnetic carbons.[15] The Cr(VI) removal capacities of the synthesized magnetic carbons were also

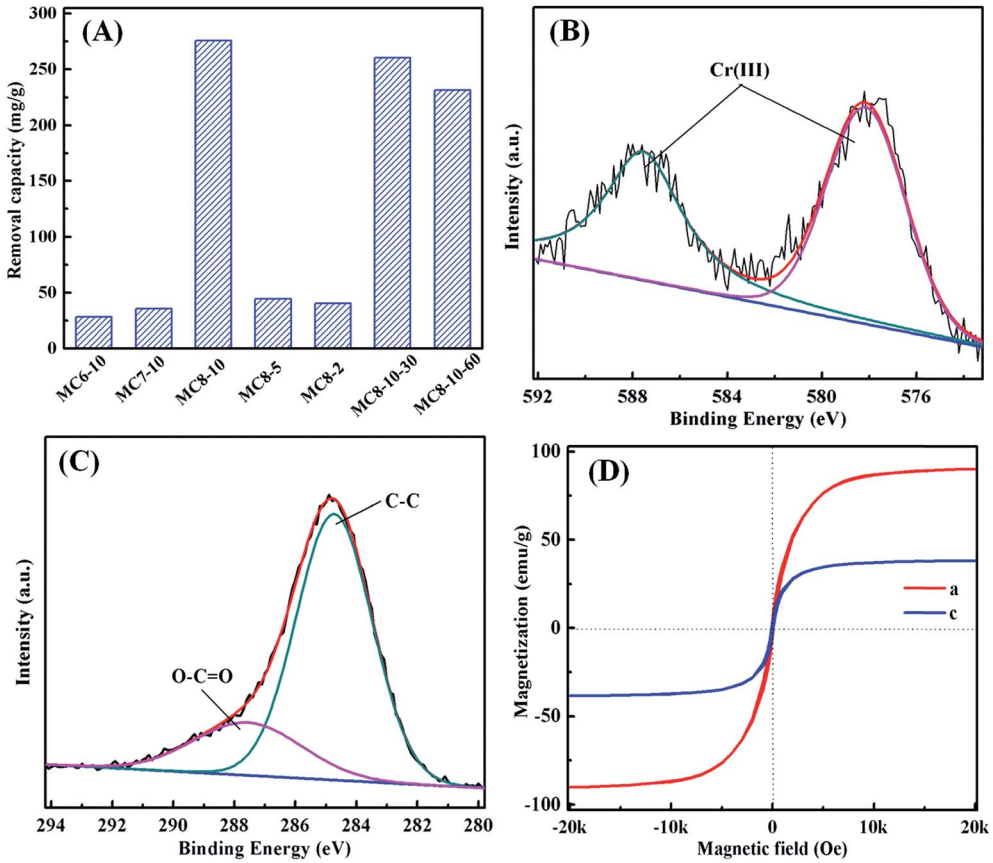

Fig. 6 (A) Cr(VI) removal by the synthesized magnetic carbons with an initial solution pH of 2.0; (B) Cr2p and (C) C1s XPS spectra of MC8–10 after being treated with Cr(VI) solution; (D) magnetic hysteresis loop of MC8–10 (a) before and (b) after being treated with Cr(VI).

determined with an initial pH of 2.0. As shown in Fig. 6A, the greatest Cr(VI) removal capacity of 278.8 mg g^{-1} was observed for MC8–10, a little higher than those of MC8–10–30 and MC8–10–60, and much higher than those of MC6–10, MC7–10, MC8–5 and MC8–2. This indicates that Cr(VI) removal by the magnetic carbon in acidic solution is highly dependent on the ZVI in the magnetic carbon. However, the removal capacity is also much higher than those of ZVI/chitosan (55.8 mg g^{-1}),[34] ZVI/Fe_3O_4 nanoparticles (186.32 mg g^{-1}),[16] and iron doped ordered mesoporous carbon (256.86 mg g^{-1}).[17]

It is interesting that the Cr(VI) removal capacities of the magnetic carbons synthesized with a final carbonization temperature of 800 °C and a heating rate of 10 °C min^{-1} (MC8–10, MC8–10–30 and MC8–10–60) are several times higher than those of the others synthesized in this study. It indicates that the ZVI in the magnetic carbons plays an important role in Cr(VI) removal from acidic solution. Moreover, the magnetic carbons with Fe_3O_4 core, including MC6–10, MC7–10, MC8–5 and MC8–2, have higher removal capacities in the acidic solution than in the neutral solution (Fig. 5A). As documented, the most important forms of Cr(VI) in aqueous solution are chromate (CrO_4^{2-}), dichromate ($Cr_2O_7^{2-}$) and hydrogen chromate ($HCrO_4^-$ and H_2CrO_4) and these ion forms are related to the solution pH.[35] The $HCrO_4^-$ is the dominant form when pH is lower than 6.8, while only CrO_4^{2-} is stable when pH is above 6.8.[4–6,13] The $HCrO_4^-$ with a higher redox potential (1.33 V) can be easily reduced to Cr(III) by the carbon layer.

MC8–10 has a higher capacity than those of MC8–10–30 and MC8–10–60 mainly due to its bigger specific surface area. MC8–10 was taken as an example to disclose the mechanisms involved in Cr(VI) in acidic solution. Fig. 6B shows the Cr2p spectra of MC8–10 after being treated with 2.0 g L^{-1} of Cr(VI) solution with an initial pH of 2.0 for 30 min. The binding energy peaks at 578.1 and 587.5 eV indicate that the adsorbed chromium was in the form of Cr(III). No Cr(VI) was detected on the surface of MC8–10, indicating that Cr(VI) was completely reduced to Cr(III). Fig. 6C shows the C1s XPS spectrum of MC8–10 after being treated with Cr(VI). The observed energy peaks at 284.7 and 288.2 eV are related to C–C and O–C=O. The newly generated O–C=O group indicates the oxidation of carbon by Cr(VI), compared to the C1s spectrum of the synthesized MC8–10 (Fig. S5†). Meanwhile, the magnetic properties of MC8-10 before and after being treated with Cr(VI) were measured (Fig. 6D). It shows that MC8–10 exhibits good magnetic properties with a saturation magnetization of 90.2 emu g^{-1}, and a sharp decrease (38.4 emu g^{-1}) was observed after being treated with an initial pH of 2.0 for 30 min, indicating that the ZVI has been consumed for Cr(VI) removal. The ZVI was dissolved by acidic solution and produced the reductive intermediates such as $H^{\bullet}$, hydrogen and Fe^{2+}, which act as electron donors for the

reduction of Cr(VI) to Cr(III).[15] The ZVI was consumed for Cr(VI) reduction and it formed precipitates of iron and chromium hydroxides on the adsorbent surface, leading to decreased magnetization. However, the magnetic carbons also exhibit a large magnetization even though they are treated with acid solutions, which can be easily separated by a permanent magnet from the solutions after being treated with Cr(VI). The ZVI has been demonstrated to show much greater Cr(VI) removal than Fe_3O_4 and Fe_2O_3 since it can provide more electrons for Cr(VI) reduction in the acidic solution. The Cr(VI) removal capacity of MC8–10 is much higher than that of the other iron related adsorbents (Table 2). Generally, the reduction of Cr(VI) to Cr(III) by the oxidation of ZVI as well as the carbon layer of the magnetic carbon was determined to be the main mechanism of Cr(VI) removal by the magnetic carbons in the acidic solution.

4. Conclusion

The magnetic carbons derived from cellulose were fabricated through a calcination method by using $Fe(NO_3)_3$ as the iron precursor. Fe^{3+} was reduced to ZVI at a carbonization temperature of 800 °C and a heating rate of 10 °C min^{-1}. The specific surface area was decreased with increasing the temperature, heating rate and retention time. The I_D/I_G of the carbon layer was increased with increasing final temperature, while was decreased with increasing retention time. MC7–10 has demonstrated the best Cr(VI) removal from neutral solution with an adsorption capacity of 22.8 mg g^{-1}. MC8–10 has a highest Cr(VI) removal capacity of 278.8 mg g^{-1} in the acidic solution due to its higher content of ZVI. The main mechanism for the Cr(VI) removal was disclosed as the reduction of Cr(VI) to Cr(III) by the oxidation of carbon in neutral solution, as well as by the oxidation of ZVI in acidic solution. Moreover, the magnetic nanoadsorbents could be easily separated from solution by using a permanent magnet after being treated with Cr(VI).

Acknowledgements

This project is financially supported by the National Science Foundation (CBET 11-37441, and CMMI 13-14486). David P. Young acknowledges support from the NSF under grant DMR 13-06392. B. Qiu acknowledges the Specific Programs in Graduate Science and Technology Innovation of Beijing Forestry University (no. BLYJ201311).

References

1 H. Gu, S. B. Rapole, Y. Huang, D. Cao, Z. Luo, S. Wei and Z. Guo, *J. Mater. Chem. A*, 2013, **1**, 2011–2021.
2 J. Zhu, S. Wei, H. Gu, S. B. Rapole, Q. Wang, Z. Luo, N. Haldolaarachchige, D. P. Young and Z. Guo, *Environ. Sci. Technol.*, 2011, **46**, 977–985.
3 C. Xu, B. Qiu, H. Gu, X. Yang, H. Wei, X. Huang, Y. Wang, D. Rutman, D. Cao and S. Bhana, *ECS J. Solid State Sci. Technol.*, 2014, **3**, M1–M9.
4 B. Qiu, J. Guo, X. Zhang, D. Sun, H. Gu, Q. Wang, H. Wang, X. Wang, X. Zhang, B. L. Weeks, S. Wei and Z. Guo, *ACS Appl. Mater. Interfaces*, 2014, **6**, 19816–19824.
5 B. Qiu, C. Xu, D. Sun, H. Wei, X. Zhang, J. Guo, W. Qiang, D. Rutman, Z. Guo and S. Wei, *RSC Adv.*, 2014, **4**, 29855–29865.
6 B. Qiu, C. Xu, D. Sun, H. Yi, J. Guo, X. Zhang, H. Qu, M. Guerrero, X. Wang, N. Noel, Z. Luo, Z. Guo and S. Wei, *ACS Sustainable Chem. Eng.*, 2014, **2**, 2070–2080.
7 A. Qian, P. Liao, S. Yuan and M. Luo, *Water Res.*, 2014, **48**, 326–334.
8 P. Mitra, D. Sarkar, S. Chakrabarti and B. K. Dutta, *Chem. Eng. J.*, 2011, **171**, 54–60.
9 N. Melitas, O. Chuffe-Moscoso and J. Farrell, *Environ. Sci. Technol.*, 2001, **35**, 3948–3953.
10 H. Gu, S. B. Rapole, J. Sharma, Y. Huang, D. Cao, H. A. Colorado, Z. Luo, N. Haldolaarachchige, D. P. Young, B. Walters, S. Wei and Z. Guo, *RSC Adv.*, 2012, **2**, 11007–11018.
11 J. Zhu, H. Gu, J. Guo, M. Chen, H. Wei, Z. Luo, H. A. Colorado, N. Yerra, D. Ding, T. C. Ho, N. Haldolaarachchige, J. Hopper, D. P. Young, Z. Guo and S. Wei, *J. Mater. Chem. A*, 2014, **2**, 2256–2265.
12 C. J. Lin, S. L. Wang, P. M. Huang, Y. M. Tzou, J. C. Liu, C. C. Chen, J. H. Chen and C. Lin, *Water Res.*, 2009, **43**, 5015–5022.
13 B. Qiu, C. Xu, D. Sun, Q. Wang, H. Gu, X. Zhang, B. L. Weeks, J. Hopper, T. C. Ho, Z. Guo and S. Wei, *Appl. Surf. Sci.*, 2014, DOI: 10.1016/j.apsusc.2014.07.039.
14 Y. Li, S. Zhu, Q. Liu, Z. Chen, J. Gu, C. Zhu, T. Lu, D. Zhang and J. Ma, *Water Res.*, 2013, **47**, 4188–4197.
15 B. Qiu, H. Gu, X. Yan, J. Guo, Y. Wang, D. Sun, Q. Wang, M. Khan, X. Zhang, B. L. Weeks, D. P. Young, Z. Guo and S. Wei, *J. Mater. Chem. A*, 2014, **2**, 17454–17462.
16 A. Rao, A. Bankar, A. R. Kumar, S. Gosavi and S. Zinjarde, *J. Contam. Hydrol.*, 2013, **146**, 63–73.
17 L. Tang, G. D. Yang, G. M. Zeng, Y. Cai, S. S. Li, Y. Y. Zhou, Y. Pang, Y. Y. Liu, Y. Zhang and B. Luna, *Chem. Eng. J.*, 2014, **239**, 114–122.
18 S. Wei, Q. Wang, J. Zhu, L. Sun, H. Lin and Z. Guo, *Nanoscale*, 2011, **3**, 4474–4502.
19 H. Gu, D. Ding, P. Sameer, J. Guo, N. Yerra, Y. Huang, Z. Luo, T. C. Ho, N. Haldolaarachchige and D. P. Young, *ECS Solid State Lett.*, 2013, **2**, M65–M68.
20 X. Zhu, Y. Liu, G. Luo, F. Qian, S. Zhang and J. Chen, *Environ. Sci. Technol.*, 2014, **48**, 5840–5848.
21 J. D. Xiao, L. G. Qiu, X. Jiang, Y. J. Zhu, S. Ye and X. Jiang, *Carbon*, 2013, **59**, 372–382.
22 D. Klemm, B. Heublein, H.-P. Fink and A. Bohn, *Angew. Chem., Int. Ed.*, 2005, **44**, 3358–3393.
23 X. Qi, L. Li, T. Tan, W. Chen and R. L. Smith, *Environ. Sci. Technol.*, 2013, **47**, 2792–2798.
24 M. Sevilla and A. B. Fuertes, *Carbon*, 2009, **47**, 2281–2289.
25 X. He, J. A. Lie, E. Sheridan and M. B. Hägg, *Ind. Eng. Chem. Res.*, 2011, **50**, 2080–2087.
26 C. N. He, F. Tian, S. J. Liu, Z. J. Du, C. J. Liu, F. Li and S. Q. Chen, *Mater. Lett.*, 2008, **62**, 3697–3699.

27 L. H. Zhang, Q. Sun, D. H. Liu and A. H. Lu, *J. Mater. Chem. A*, 2013, **1**, 9477–9483.
28 X. Zhu, Y. Liu, C. Zhou, G. Luo, S. Zhang and J. Chen, *Carbon*, 2014, **77**, 627–636.
29 H. Wang, Z. Xu, H. Yi, H. Wei, Z. Guo and X. Wang, *Nano Energy*, 2014, **7**, 86–96.
30 D. McIntosh, V. N. Khabashesku and E. V. Barrera, *J. Phys. Chem. C*, 2007, **111**, 1592–1600.
31 J. Cheng, P. R. Chang, P. Zheng and X. Ma, *Ind. Eng. Chem. Res.*, 2014, **53**, 1415–1421.
32 B. Qiu, X. Cheng and D. Sun, *Bioresour. Technol.*, 2012, **113**, 102–105.
33 D. Park, Y. S. Yun and J. M. Park, *J. Colloid Interface Sci.*, 2008, **317**, 54–61.
34 N. N. Thinh, P. T. B. Hanh, L. T. T. Ha, L. N. Anh, T. V. Hoang, V. D. Hoang, L. H. Dang, N. V. Khoi and T. D. Lam, *Mater. Sci. Eng., C*, 2013, **33**, 1214–1218.
35 X. F. Sun, Y. Ma, X. W. Liu, S. G. Wang, B. Y. Gao and X. M. Li, *Water Res.*, 2010, **44**, 2517–2524.
36 J. Hu, G. Chen and I. M. C. Lo, *Water Res.*, 2005, **39**, 4528–4536.
37 J. Hu, I. M. C. Lo and G. Chen, *Sep. Purif. Technol.*, 2007, **58**, 76–82.
38 Z. Fang, X. Qiu, R. Huang, X. Qiu and M. Li, *Desalination*, 2011, **280**, 224–231.